Title	Millennial-scale hydrographic changes in the northwestern Pacific during marine isotope stage 19: teleconnections with ice melt in the North Atlantic
Authors	Yuki Haneda, Makoto Okada, Yoshimi Kubota, Yusuke Suganuma
Citation	Earth and Planetary Science Letters, 531, 1-12, 2019
Issue Date	2020-3-15
Type	Journal Article
URL	https://doi.org/10.1016/j.epsl.2019.115936
Right	
Textversion	publisher

Earth and Planetary Science Letters ••• (••••) ••••••

Contents lists available at ScienceDirect

Earth and Planetary Science Letters

www.elsevier.com/locate/epsl

Millennial-scale hydrographic changes in the northwestern Pacific during marine isotope stage 19: Teleconnections with ice melt in the North Atlantic

Yuki Haneda [a,b,*], Makoto Okada [b], Yoshimi Kubota [c], Yusuke Suganuma [a,d]

[a] National Institute of Polar Research, 10-3 Midori-cho, Tachikawa, Tokyo 190-8518, Japan
[b] Department of Environmental Science, Ibaraki University, 2-1-1 Bunkyo, Mito, Ibaraki 310-8512, Japan
[c] Department of Geology and Paleontology, National Museum of Nature and Science, 4-1-1 Amakubo, Tsukuba, Ibaraki, 305-0005, Japan
[d] Department of Polar Science, School of Multidisciplinary Sciences, The Graduate University for Advanced Studies (SOKENDAI), Midori-cho 10-3, Tachikawa, Tokyo 190-8518, Japan

ARTICLE INFO

Article history:
Received 24 March 2019
Received in revised form 12 August 2019
Accepted 27 October 2019
Available online xxxx
Editor: L. Robinson

Keywords:
marine isotope stage (MIS) 19
oxygen stable isotope
climatic teleconnection
northwestern Pacific Ocean
Kuroshio Extension Front
Chiba composite section

ABSTRACT

Marine isotope stage (MIS) 19 has been suggested as the best orbital analogue of the present interglacial period. Thus, its paleoenvironmental reconstruction will provide valuable information on future climate change, excluding anthropogenic impacts. The Kuroshio Current, the largest western boundary current in the northwestern Pacific, transports large amounts of heat and water poleward and strongly influences both East Asian and global climates. However, the responses of the Kuroshio Current to the variable intensity of the Atlantic meridional overturning circulation (AMOC) under this orbital configuration remain unknown. Here, we provide new centennial-scale resolution oxygen isotope ($\delta^{18}O$) records throughout MIS 19 using benthic, as well as subsurface and surface planktonic foraminifera from the Chiba composite section, a marine succession sequence in central Japan, to reconstruct detailed paleoceanographic variations in the northwestern Pacific and reveal the response of the Kuroshio Current to climate variability in the North Atlantic under this orbital configuration. The vertical water temperature structure and its gradient (ΔT) based on $\delta^{18}O$ profiles elucidates the latitudinal oscillations of the Kuroshio Extension Front (KEF) on a millennial scale during the late MIS 19 and MIS 20–19 transition in association with AMOC disruption/reactivation due to freshwater discharges into the North Atlantic. The power spectra of the surface $\delta^{18}O$ and ΔT show half-precession periodicity throughout MIS 19, which probably originated from equatorial insolation at equinoxes co-occurring with the orbital perihelion. This periodicity was especially strong during MIS 19c, during which paleoceanographic records from the North Atlantic show minor variations in the AMOC and freshwater discharge. Our results suggest that millennial-scale oceanographic variation and stability along the KEF under this orbital configuration are influenced by both North Atlantic climate variability and tropical insolation forcing.

1. Introduction

Paleoclimatic records from Greenland and the sub-polar North Atlantic have documented millennial-scale climate variations (e.g., Heinrich, 1988; Bond et al., 1993; Dansgaard et al., 1993). The millennial-scale climate changes during the last glacial period are thought to have been generated by internal dynamics (e.g., atmospheric, oceanic, and ice-sheet dynamics) (Clement and Peterson, 2008; Alvarez-Solas et al., 2013; Menviel et al., 2014), and modulated by external forces (insolation modulated by the Milankovich cycle) (Short et al., 1991; Berger et al., 2006). Several studies on the last glacial period, based on paleoproxies and model simulations (e.g., Henry et al., 2016), have indicated that melting of the Northern Hemisphere ice-sheet and the resulting freshwater discharge into the North Atlantic accelerated the slowdown or shutdown of the Atlantic meridional overturning circulation (AMOC), which consists of a northward upper limb and a southward lower limb associated with deep water formation in the sub-polar North Atlantic, and caused abrupt global climate changes to occur. This climate variability due to freshwater forcing prevailed throughout the Northern Hemisphere via atmospheric dynamics (Broccoli et al., 2006; Clement and Peterson, 2008; Asmerom et al., 2010) and in Antarctica via the thermal bipolar

* Corresponding author at: National Institute of Polar Research, 10-3 Midori-cho, Tachikawa, Tokyo 190-8518, Japan.
E-mail address: yuuki.haneda.paleo@gmail.com (Y. Haneda).

https://doi.org/10.1016/j.epsl.2019.115936

seesaw mechanism (Stocker and Johnsen, 2003). These suggested mechanisms of abrupt climate change based on paleoproxies and model simulations provide valuable information that can be employed to depict future climate changes.

Marine Isotope Stage (MIS) 19, spanning from 761 to 790 ka (Lisiecki and Raymo, 2005), has been suggested as the best orbital analog for the present interglacial period (MIS 1). This is because the orbital configurations during the two interglacial periods are characterized by similar phasing of obliquity maxima with precession minima and low eccentricity (Tzedakis et al., 2012). Therefore, climate changes during MIS 19 are thought to provide essential information that can be utilized to distinguish present and future climate changes due to anthropogenic greenhouse gas emissions from orbitally controlled natural climate change. Millennial-scale climate changes have been documented during the MIS 20–19 transition (Termination IX: T-IX) and late MIS 19 in paleoclimatic and paleoceanographic records from the North Atlantic (Kleiven et al., 2011; Ferretti et al., 2015; Sánchez Goñi et al., 2016), Indian Ocean (Valet et al., 2014), land sections in Italy (Giaccio et al., 2015; Simon et al., 2017; Nomade et al., 2019; Regattieri et al., 2019), the Osaka Bay (Hyodo et al., 2017) and Chiba, Japan (Suganuma et al., 2018), Lake El'gygytgyn in far East Russia (Wennrich et al., 2014), Lake Baikal in southeastern Russia (Prokopenko et al., 2006), and Antarctica (Jouzel et al., 2007). The general consistencies of the amplitudes and timing of these millennial-scale variations suggest a global climatic teleconnection linked to North Atlantic ice-sheet dynamics during these periods (Tzedakis et al., 2012; Nomade et al., 2019).

The North Pacific Ocean contains the Kuroshio Current (Fig. 1b), which strongly affects East Asian and global climates by transporting large amounts of heat and water from low to middle latitudes (e.g., Kida et al., 2016). Isono et al. (2009) argued that the North Pacific Subtropical Gyre and Kuroshio Current responded to abrupt climate changes in the North Atlantic on a millennial scale during the Holocene. However, the Holocene record is not sufficiently long to elucidate the behavior of the North Pacific during the entire interglacial period under an orbital configuration characterized by phasing of obliquity maxima with precession minima and low eccentricity.

In this study, we provide new centennial-scale resolution oxygen isotope records obtained from benthic and, subsurface and surface planktonic foraminifera from the terrestrially exposed Chiba composite section (CbCS) to reconstruct the detailed paleoceanographic variations in the northwestern Pacific during MIS 19 under this orbital configuration. The CbCS is located in central Japan and faces the northwest Pacific Ocean, which contains the Kuroshio Extension and Subarctic fronts, which generate a distinct temperature–salinity gradient (Fig. 1b). The CbCS is a continuous marine succession sequence ranging from the late MIS 20 to early MIS 18. Its sedimentation rate, which varies between 0.44 and 3.87 m in association with eustatic sea level changes, is sufficiently high to observe millennial-scale climatic changes using well-preserved marine microfossils and pollen records (Okada et al., 2017; Suganuma et al., 2018). Therefore, our oxygen isotope records obtained using multiple species of foraminifera can provide a centennial-scale resolution time series of the vertical water temperature structure variation in the CbCS that can be utilized to evaluate the impact of AMOC variability on the Kuroshio Current in the northwestern Pacific under weak precession forcing.

2. Background information

2.1. Modern oceanographic setting of the northwestern Pacific Ocean

The Kuroshio Current, which is the major western boundary current in the northwestern Pacific, is an offshoot of the North Equatorial Current in the wind-driven North Pacific Subtropical Gyre and has important effects on East Asian and global climates associated with northward thermal transport. The Kuroshio Current flows northward along the continental shelf in the Okinawa Trough (Figs. 1a and b) and subsequently flows along the southern coast of Japan (Fig. 1b; Qiu, 2001). Off the Boso Peninsula around 35°N, the current leaves the coast of Japan and travels eastward as the Kuroshio Extension Current (KEC), which generates the Kuroshio Extension Front (KEF) just to the north of its axis (Fig. 1b). The mean axis of the KEC between 140°E and 160°E is displaced between 33.5°N and 35.5°N on an interannual scale (Qiu, 2001). The modern annual mean sea surface temperature (SST) and salinity (SSS) of the Kuroshio Current off central Japan are 19–21 °C and 34, respectively, at 35.5–36.5°N (Figs. 1b and S1; Locarnini et al., 2013; Zweng et al., 2013). Based on modern observations, southward latitudinal SST and SSS gradients across the Kuroshio Extension are $+0.7 \pm 0.2$ (in August) to $+1.8 \pm 0.7$ (in December) °C/100 km and -0.10 (in March) to -0.19 (in September) salinity/100 km, respectively (Kida et al., 2016).

In contrast, the Oyashio Current is a western boundary current in the wind-driven North Pacific Subpolar Gyre (Fig. 1a; Qiu, 2001). The Oyashio flows along the coast of Hokkaido and splits into two paths. One veers east-northeastward at 42°N as the Subarctic Current generating the Subarctic Front (SAF), and the other veers southward along Japan as the first Oyashio intrusion (Fig. 1b). The annual mean latitude of the southern edge of the Oyashio intrusion is 38.7°N, although this fluctuates between 37°N and 41°N on an interannual scale (Qiu, 2001). The modern annual mean SST and SSS of the Oyashio Current off northern Japan are 6–8 °C and 33.0, respectively, at 42.5–43.5°N (Figs. 1b and S1; Locarnini et al., 2013; Zweng et al., 2013). Based on modern observations, southward latitudinal SST and SSS gradients across the Subarctic Current are $+2.0 \pm 1.5$ (in October) to $+3.3 \pm 0.4$ (in April) °C/100 km and -0.35 (in April and December) to -0.54 (in September) salinity/100 km, respectively (Kida et al., 2016).

In the modern North Pacific, southward displacement of oceanic fronts is induced by intensification and southward shifting of the prevailing westerly winds and generates a negative SST anomaly at the subpolar front (e.g., Kwon et al., 2010). The southward shift of the prevailing westerlies is likely linked to the decadal variability of the Aleutian Low, which develops around Aleutian Island in the North Pacific during the winter, because of a high correlation between the enhanced (weakened) surface Aleutian low and a negative (positive) SST anomaly along the SAF (Taguchi et al., 2012).

2.2. Geological setting

The CbCS is a well-exposed marine succession sequence within the Kokumoto Formation, Kazusa Group, and crops out in the central part of the Boso Peninsula (Fig. 1c). The CbCS consists of five sections: the Yoro River (35°17.41′N; 140°08.48′E), Yoro-Tabuchi (35°17.41″N; 140°08.49′E), Yanagawa (35°17.15′N; 140°07.88′E), Urajiro (35°16.85′N; 140°07.47′E), and Kokusabata (35°18.52′N; 140°11.89′E) sections (Figs. 1c and S2; Suganuma et al., 2018). The Chiba section, a candidate of Global Boundary Stratotype Section and Point of the Lower–Middle Pleistocene boundary, is included in the lowermost part of the Yoro River section. The lithofacies of the middle part of the CbCS is dominated by bioturbated silty beds with minor sandy beds and shows no evidence of episodic deposition (Nishida et al., 2016), although thick sandy beds are observable in the lowermost and upper parts of the CbCS (Figs. 2 and S2). In addition to detailed field observations, trace fossil assemblages indicate that the CbCS was deposited in a continental slope environment below 200 m water depth (Nishida et al., 2016). Numerous tephra beds (Ku1, Ku2A, Ku2B, Tas, Tap, and Byk) have been observed in the CbCS and facilitate detailed correlations be-

Please cite this article in press as: Haneda, Y., et al. Millennial-scale hydrographic changes in the northwestern Pacific during marine isotope stage 19: Teleconnections with ice melt in the North Atlantic. Earth Planet. Sci. Lett. (2019), https://doi.org/10.1016/j.epsl.2019.115936

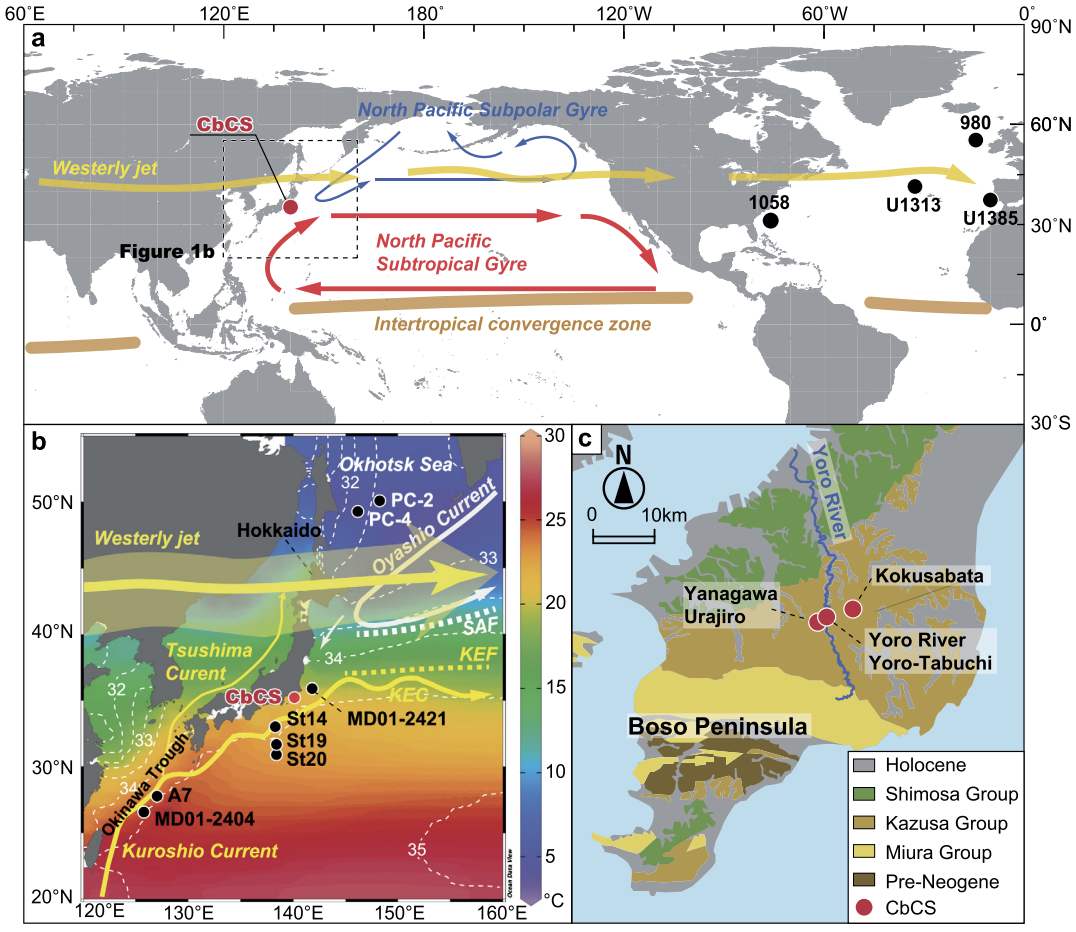

Fig. 1. Location of the CbCS and its atmospheric and oceanographic context. (a) Locations of the Westerly Jet in summer, the ITCZ, and the marine records discussed in the text. These references include: ODP Site 980 (Wright and Flower, 2002) and Site 1058 (Weirauch et al., 2008; Billups and Scheinwald, 2014), and IODP Sites U1313 (Ferretti et al., 2015) and U1385 (Sánchez Goñi et al., 2016). (b) Current oceanographic and atmospheric context around Japan and marine records discussed in the text. The positions of the major ocean currents are based on Qiu (2001). The annual mean ocean temperature and salinity gradients are from the World Ocean Atlas 2013 (Locarnini et al., 2013; Zweng et al., 2013) drawn using Ocean Data View software (Schlitzer, 2015). These references include A7 (Sun et al., 2005); MD01-2404 (Chen et al., 2010); MD01-2421 (Yamamoto et al., 2005; Oba et al., 2006); PC-2 and PC-4 (Seki et al., 2004); and St 14, 19, and 20 (Sawada and Handa, 1998). (c) Simplified geological map of the Boso Peninsula. Modified from Suganuma et al. (2018). CbCS: Chiba composite section. KEF: Kuroshio Extension Front, SAF: Subarctic Front.

tween the sections (Fig. S1; Suganuma et al., 2018). Based on local tephrostratigraphy, the thickness scales of the lithostratigraphies along the Urajiro, Yanagawa, and Kokusabata sections were converted into that of the Yoro River section (Figs. 2 and S2; Suganuma et al., 2018).

2.3. Chronological framework of the CbCS

The U-Pb radiometric age of the Byk-E tephra (Suganuma et al., 2015), stratigraphic position of the Matuyama–Brunhes (M–B) boundary (Okada et al., 2017; Simon et al., 2019), and benthic $\delta^{18}O$ stratigraphy (Suganuma et al., 2018) provide a robust chronological framework for dating the CbCS. The Byk-E tephra is intercalated with a continuous silty unit (Fig. S2) and its U-Pb radiometric age was determined to be 772.7 ± 7.2 ka (Suganuma et al., 2015). The M–B boundary was observed 1.1 m above the Byk-E tephra in the Yoro River section (Fig. 2; Okada et al., 2017), and its astronomically tuned age was dated as 772.9 ka (Fig. S3; Suganuma et al., 2018; Simon et al., 2019). The latest age model was proposed based on the astronomically tuned benthic $\delta^{18}O$ stratigraphy obtained from the Yanagawa, Urajiro, and Kokusaba sections at 1 m spacing, and partially from the Yoro River and Yoro-Tabuchi sections at 20 cm to 1 m spacing (Suganuma et al., 2018). They graphically correlated the benthic $\delta^{18}O$ profile of the CbCS with a sea level proxy curve obtained from Ocean Drilling Project (ODP) Site 1123 off New Zealand (Elderfield et al., 2012), with assistance from the U-Pb radiometric age of the Byk-E tephra (Suganuma et al., 2015) and the stratigraphic position of the M–B boundary (Okada et al., 2017), which occurred just after the MIS 19 maximum (Channell et al., 2010; Valet et al., 2019).

3. Material and methods

3.1. Oxygen isotope analyses

We conducted new foraminiferal $\delta^{18}O$ analyses to improve the temporal resolution of the $\delta^{18}O$ records of the CbCS. Siltstone samples were collected from the Yoro River and Yoro-Tabuchi sections in 10–20 cm intervals from −14.6 m to the 13.5 m horizon above the Byk-E tephra bed and in 50 cm intervals above this, ranging up to the 95.5 m horizon, yielding a total of 328 samples in combination with 86 existing samples from Okada et al. (2017) and Suganuma et al. (2018) (Figs. 2 and S2). Prior to handpicking fossil foraminifera, the siltstone samples were disaggregated using Na_2SO_4, and the non-magnetic fraction was isolated from the magnetic fraction using a Frantz magnetic isodynamic separator at Ibaraki University. The $\delta^{18}O$ compositions were measured using benthic species *Cibicides aknerianus* and *Bolivinita quadrilatera* from the >250 μm size fractions and planktonic species *Globorotalia inflata* and *Globigerina bulloides* from the >250 μm and 150–250 μm

Please cite this article in press as: Haneda, Y., et al. Millennial-scale hydrographic changes in the northwestern Pacific during marine isotope stage 19: Teleconnections with ice melt in the North Atlantic. Earth Planet. Sci. Lett. (2019), https://doi.org/10.1016/j.epsl.2019.115936

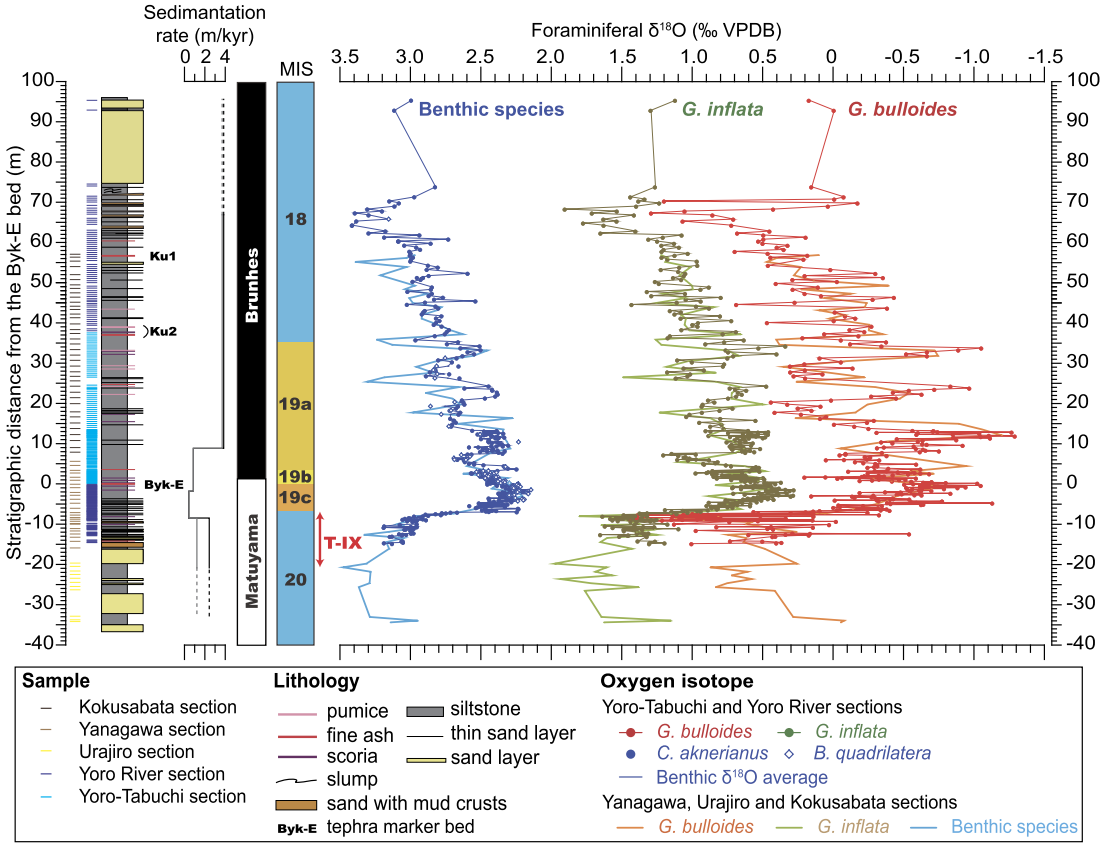

Fig. 2. Benthic and planktonic δ^{18}O profiles on a thickness scale. The composite lithologic column was obtained based on Fig. S2. Sedimentation rates were calculated using the age model and thickness of the section with (black line) and without (gray line) sandy layers (Suganuma et al., 2018). Polarity is from Okada et al. (2017). The low-resolution δ^{18}O profiles with 100 cm spacing from the Urajiro, Yanagawa, and Kokusabata sections are shown as light blue (benthic species), light green (*G. inflata*), and orange thick lines (*G. bulloides*). The ultrahigh-resolution δ^{18}O profiles with 10–50 cm spacing are shown as open blue diamonds (benthic species *B. quadorilatera*), and closed blue (benthic species *C. aknerianus*), closed green (*G. inflata*) and closed red circles (*G. bulloides*). MIS: marine isotope stage, T-IX: Termination IX, VPDB: Vienna Pee Dee Belemnite. (For interpretation of the colors in the figure(s), the reader is referred to the web version of this article.)

size fractions. Twenty or more individual planktonic foraminiferal tests were used for most measurements, although fewer than 20 individuals were used for a few planktonic species measurements when the abundance of this species was low. More than three individuals of the benthic species were used for measurements. The analyses were performed using a Finnigan-MAT253 isotope mass spectrometer coupled with a Kiel IV carbonate preparation device in the Department of Geology and Paleontology at the National Museum of Nature and Science. NBS-19 and JCp-1 (Coral *Porites* sp.) were used as working standards to calibrate the measured isotope values to the Vienna Pee Dee Belemnite. The standard deviation of δ^{18}O was calculated as 0.033‰ based on 376 measurements of NBS-19 standard specimens.

To correct an interspecies δ^{18}O offset between *C. aknerianus* and *B. quadrilatera*, we extracted 33 set of these benthic species, which co-exist in the same sample horizons. The average of the difference between their benthic δ^{18}O values is 0.65 ± 0.10‰ (error is a standard deviation), which is consistent with the δ^{18}O offset between *B. quadrilatera* and *Cibicidoides* (0.64‰) in Suganuma et al. (2015). We corrected the δ^{18}O of *C. aknerianus* analyzed in this study to that of *B. quadrilatera* by adding 0.65‰, and also applied this interspecies calibration to previous benthic δ^{18}O data obtained from the Yoro River and Yoro-Tabuchi sections by Okada et al. (2017) and Suganuma et al. (2018) to maintain consistency.

Abundance of *G. bulloides* is thought to be primarily controlled by variations in primary production (Schiebel and Hemleben, 2017), and the amount of chlorophyll-α is the largest in winter in the Kuroshio Current (e.g., Imai et al., 1988). A large flux of *G. bulloides* was observed mainly at depths shallower than 100 m from autumn to spring in the Kuroshio region (Yamasaki and Oda, 2003; Xu et al., 2005; Yamasaki et al., 2010). The deep-dwelling planktonic species *G. inflata* is abundant in winter or spring independent of temperature and productively (e.g., Jonker and Kucera, 2015). Paleothermometry based on Mg/Ca ratios of foraminiferal tests infers that *G. inflata* forms its test at depths of 300–400 m in the subtropical North Pacific, where temperature shows no seasonal variation (Sagawa et al., 2011). Therefore, the δ^{18}O components of *G. inflata* and *G. bulloides* likely reflect the calcification temperature and salinity at habitat depths in colder seasons.

3.2. Age model

In this study, we used the latest age model for the CbCS proposed by Suganuma et al. (2018) to convert the δ^{18}O profiles from thickness to age scales (Fig. S3). The resulting age interval of the new δ^{18}O record is 747.6–801.1 ka, and the average temporal resolution is ~160 yr (Fig. S3). However, the age model of the CbCS includes an uncertainty of at least 4 kyr due to the chronologic uncertainty of the LR04 stack used as a target curve by Elderfield et al. (2012) (Lisiecki and Raymo, 2005).

3.3. Assignment of substages in MIS 19

MIS 19 has been divided into three substages: MIS 19c, 19b, and 19a, in chronological order (Railsback et al., 2015). Suganuma et al. (2018) assigned the inceptions of MISs 19 and 18 following

Lisiecki and Raymo (2005), and defined the substage boundaries of MIS 19 based on low-resolution benthic $\delta^{18}O$ records with a partial high-resolution record of the CbCS. The previous assignment of substages, however, should be redefined based on new centennial-resolution $\delta^{18}O$ records, which reveal millennial-scale paleoceanographic variations. Nomade et al. (2019) proposed a stratigraphic scheme for assigning substages in MIS 19 based on climatic variability: MIS 19c corresponds to the climatically stable part of stage 19; MIS 19b corresponds to the first climatic cooling; and MIS 19a corresponds to the most unstable part of stage 19. Following this definition, we reassigned the stage boundaries in the CbCS oxygen isotope stratigraphy based on the new centennial-resolution benthic $\delta^{18}O$ record. Astronomical ages for each stage and substage boundaries are estimated as 787.5 ka (MIS 20/19c at the −6.74 m horizon), 773.9 ka (MIS 19c/19b at the 0.20 m horizon), 770.1 ka (MIS 19b/19a at the 3.58 m horizon) and 756.9 ka (MIS 19a/18 at the 35.25 m horizon) based on the latest age model of Suganuma et al. (2018) (Figs. 2 and S3).

3.4. Time-series analyses

We performed spectral and wavelet analyses to assess statistically significant cycles of the millennial-scale components in the $\delta^{18}O$ records. The spectral analysis was conducted according to the methods of Schulz and Mudelsee (2002), which can be employed to test whether spectral peaks in a time series are significant against the red-noise background, using the PAST software (Hammer et al., 2001). Wavelet analysis using the Morlet wavelet, which decomposes a time series into time-frequency space, was conducted using a MATLAB software package by Torrence and Compo (1998). Prior to the spectral analyses, we removed the obliquity and centennial components from the measured $\delta^{18}O$ records to highlight any millennial-scale spectra using the following procedures:

- First, the measured $\delta^{18}O$ records were spaced out evenly at a temporal resolution of 200 yr by linear interpolation using the Analyseries software (Paillard et al., 1996).
- Second, we performed Gaussian bandpass filtering to extract the 0.024 kyr^{-1} frequency with a bandwidth of 0.05 for the 200 yr-spaced $\delta^{18}O$ records.
- Third, the millennial component of the $\delta^{18}O$ records was estimated by subtracting the bandpass filter output curve from the 200 yr-spaced $\delta^{18}O$ records.
- Finally, the millennial components of the $\delta^{18}O$ records were smoothed by a five-point moving average to avoid the influence of frequencies larger than the Nyquist frequency ($1/2\Delta t$, where Δt is the temporal resolution of the record).

We then performed the time series analyses using the resulting millennial components of each $\delta^{18}O$ record.

4. Results

4.1. Oxygen isotope records and vertical temperature gradient

The ultrahigh-resolution $\delta^{18}O$ profiles on a thickness scale are shown together with the low-resolution profiles in Fig. 2. The timing and amplitude of the variations in the new ultrahigh-resolution $\delta^{18}O$ profiles for benthic ($\delta^{18}O_{Ben}$), *G. inflata* ($\delta^{18}O_{inf}$), and *G. bulloides* ($\delta^{18}O_{bul}$) on few-meter and dozen-meter scales are generally consistent with those of the low-resolution $\delta^{18}O$ profiles (Fig. 2). The low-resolution $\delta^{18}O_{Ben}$ from the Kokusabata section above the 15 m horizon above the Byk-E tephra bed, however, are intermittently ∼0.2–0.4‰ higher than the ultrahigh-resolution $\delta^{18}O_{Ben}$ from the Yoro River and Yoro-Tabuchi sections, while the values of $\delta^{18}O_{Ben}$ from the Yanagawa and Urajiro sections are consistent with those from the sections along the Yoro River. On the other hand, both the ultrahigh- and low-resolution planktonic $\delta^{18}O$ records show comparable variations in terms of both timing and amplitude between each section of the CbCS.

The $\delta^{18}O_{Ben}$, $\delta^{18}O_{inf}$, and $\delta^{18}O_{bul}$ profiles were basically described as synchronous variations on an orbital scale on which millennial-scale variations were superimposed (Fig. 3). $\delta^{18}O_{Ben}$ varies between 2.14‰ and 3.47‰, as does that of the LR04 stack (Lisiecki and Raymo, 2005), although the average $\delta^{18}O_{Ben}$ value within the study interval (2.65‰) is ∼1.5‰ lower than that of the LR04 stack (4.15‰). $\delta^{18}O_{inf}$ varies between 0.27‰ and 1.97‰ on the glacial–interglacial cycle scale, and its average within the study interval is 0.93‰, which is an intermediate value between the three $\delta^{18}O$ records. $\delta^{18}O_{bul}$ varies between −1.30‰ and 1.43‰, and its average within the study interval is −0.10‰.

The millennial-scale oscillation that occurred during the late MIS 19 exhibits four stadial and four interstadial periods (Fig. 3). The average amplitude of the millennial-scale oscillation in the $\delta^{18}O_{bul}$ profile (∼1.2‰) is much larger than those in the $\delta^{18}O_{inf}$ (∼0.7‰) and $\delta^{18}O_{Ben}$ (∼0.4‰) profiles. This indicates that the millennial-scale oscillation originated from changes in water properties of the surface water. The sensitivity of $\delta^{18}O$ in a foraminiferal carbonate test ($\delta^{18}O_{carb}$) to water temperature and salinity changes were determined as −0.23‰/°C (Erez and Luz, 1983) and +0.52‰/salinity (Oba et al., 2006), respectively. Based on these sensitivities and modern observations across the KEF, southward latitudinal gradients of $\delta^{18}O_{carb}$ sensitivities to SST and SSS are calculated as −0.16 to −0.41‰/100 km, and as +0.05 to +0.10‰/100 km, respectively. Therefore, we infer that the effect of water temperature on $\delta^{18}O_{carb}$ is larger than that of salinity in the KEF region. Freshwater input from local rivers or local rainfall over the KEF region might cause a SSS change, but it is unlikely in the case of marine plankton assemblages in the CbCS; the marine plankton assemblages in the CbCS show no evidence for large variations in the SSS (Suganuma et al., 2018). The relative abundance of the planktonic foraminifer *Turborotalia quinqueloba* showed high percentages (∼50%) during the last deglaciation, associated with a large freshwater discharge from the Chinese continent that was closely related to the low-salinity water (Xu and Oda, 1999). The relative abundance of this species in the CbCS is low (0–0.42%) throughout MIS 19 and is not associated with the $\delta^{18}O$ variations (Suganuma et al., 2018). Moreover, freshwater planktonic diatoms in the TB-2 sediment core are also less abundant (0–4.3%) (Tanaka et al., 2017). Based on these records, there was likely no freshwater event that occurred across the CbCS, and thus the millennial-scale variations in the $\delta^{18}O$ profiles of the CbCS mainly originated from SST changes in the northwestern Pacific.

We named the millennial-scale $\delta^{18}O$ variations during late MIS 19, which are interpreted as reflecting SST variability, Millennial Isotopic Oscillations (MIOs), and labeled the stadial and interstadial periods MIO-Stadial 1 (MIO-S1) to MIO-S4 and MIO-Interstadial 1 (MIO-I1) to MIO-I4, in chronological order (Fig. 3). The boundary ages for each period were defined at the mid-points of rapid warming and cooling intervals based on $\delta^{18}O_{bul}$. The durations of the MIO cycles (from an interstadial period to the next stadial period) attenuated from 5.3 kyr to 2.6 kyr toward MIS 18 (Fig. 3).

To clarify the temporal variations in the vertical water temperature profile, the difference in water temperature between the surface and bottom water (ΔT) was calculated by subtracting $\delta^{18}O_{bul}$ from $\delta^{18}O_{Ben}$. These values were converted into temperatures based on the sensitivity of $\delta^{18}O_{carb}$ to water temperature change (−0.23 ‰/°C, from Erez and Luz, 1983) (Fig. 3d). Modern vertical profiles of salinity off the Boso Peninsula vary between 34.2 (at a depth of ∼600 m) and 34.6 (at a depth of ∼100 m)

Please cite this article in press as: Haneda, Y., et al. Millennial-scale hydrographic changes in the northwestern Pacific during marine isotope stage 19: Teleconnections with ice melt in the North Atlantic. Earth Planet. Sci. Lett. (2019), https://doi.org/10.1016/j.epsl.2019.115936

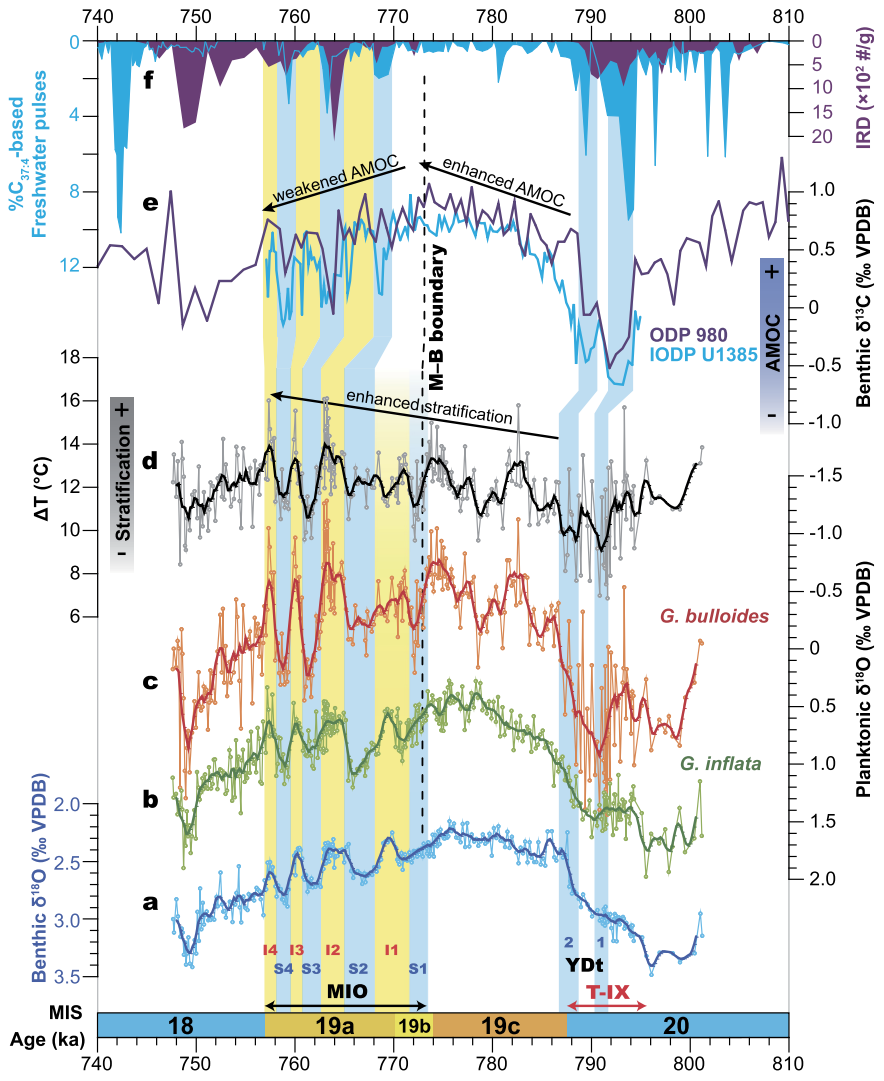

Fig. 3. Comparison of the $\delta^{18}O$ records and vertical water temperature gradient from the CbCS and paleoceanographic records from the North Atlantic. (a–c) Measured $\delta^{18}O$ record and 1000 yr moving average profile for benthic species (light blue open circle and thin line, and thick blue line), subsurface planktonic species *G. inflata* (light green open circle and thin line, and green thick line), and surface planktonic species *G. inflata* (orange open circle and thin line, and red thick line). (d) Profile of ΔT between surface and bottom water in the CbCS (gray open circle and thin line) and 1000 yr moving average (black thick line). (e) Benthic $\delta^{13}C$ records from ODP Site 980 (purple line; Wright and Flower, 2002) and IODP Site U1385 (light blue line; Sánchez Goñi et al., 2016). (f) $\%C_{37:4}$-based freshwater pulse from IODP Site U1385 (light blue shaded area; Sánchez Goñi et al., 2016; Rodrigues et al., 2017) and IRD records from ODP Site 980 (purple shaded area; Wright and Flower, 2002). The vertical light blue and yellow shaded regions indicate the stadial and interstadial periods, respectively, correlated between the CbCS and North Atlantic paleoceanographic records. The vertical black dashed line indicates the correlation of the M–B boundary between the CbCS and ODP Site 980. AMOC: Atlantic Meridional Overturning Circulation, M–B boundary: Matuyama–Brunhes boundary, MIO: Millennial Isotopic oscillation, MIS: marine isotope stage, T-IX: Termination IX, VPDB: Vienna Pee Dee Belemnite, YDt: Younger Dryas-type cooling sub-event.

(Zweng et al., 2013) and the effect of vertical change in salinity on $\delta^{18}O_{carb}$ is calculated as 0.21‰ (Oba et al., 2006), corresponding to a water temperature variation of 0.9 °C. The effect of vertical salinity change for $\delta^{18}O_{carb}$ is much less than that of vertical water temperature change (Fig. S1). The average ΔT during MIS 19c was 12.0 °C, which is similar to the modern ΔT from 100 to 500 m water depth. The deduced paleodepth for the CbCS is consistent with the paleodepth estimate based on detailed lithologic observations and trace fossil assemblage analysis (Nishida et al., 2016). The radiolarian assemblage analysis from the CbCS revealed deep-dwelling species, which supports our paleodepth estimation (Suganuma et al., 2018). Therefore, the ΔT represents the vertical temperature gradient between the surface and approximately 500 m water depth.

The long-term trend of the ΔT profile throughout MIS 19 is very similar to the long-term increments in the planktonic foraminiferal assemblage-based SST and the abundance of *Florisphaera profunda* in the CbCS. This species is an abundant type of calcareous nannoplankton in the lower photic zone in the modern North Pacific (Suganuma et al., 2018). These previous observations indicate a gradual SST warming and the enhancement of ocean surface stratification in the CbCS from MIS 19 to MIS 18 (Suganuma et al., 2018), which support our interpretation of ΔT variations exhibiting enhanced or weakened stratification.

The ΔT profile shows two minimum values at 791.0 and 788.4 ka during T-IX (Fig. 3d). On the other hand, $\delta^{18}O$ profiles show only one cooling period interrupting T-IX (Figs. 3a–c). Suganuma et al. (2018) reported that a Younger Dryas-type (YDt) cooling event occurred during T-IX and implied that the YDt cooling event consisted of two short-term cooling sub-events, which have been globally documented in paleoproxies. We numbered these weakened stratification events during T-IX YDt sub-events 1 and 2 (YDt-1 and YDt-2, respectively), in chronological order (Fig. 3).

Please cite this article in press as: Haneda, Y., et al. Millennial-scale hydrographic changes in the northwestern Pacific during marine isotope stage 19: Teleconnections with ice melt in the North Atlantic. Earth Planet. Sci. Lett. (2019), https://doi.org/10.1016/j.epsl.2019.115936

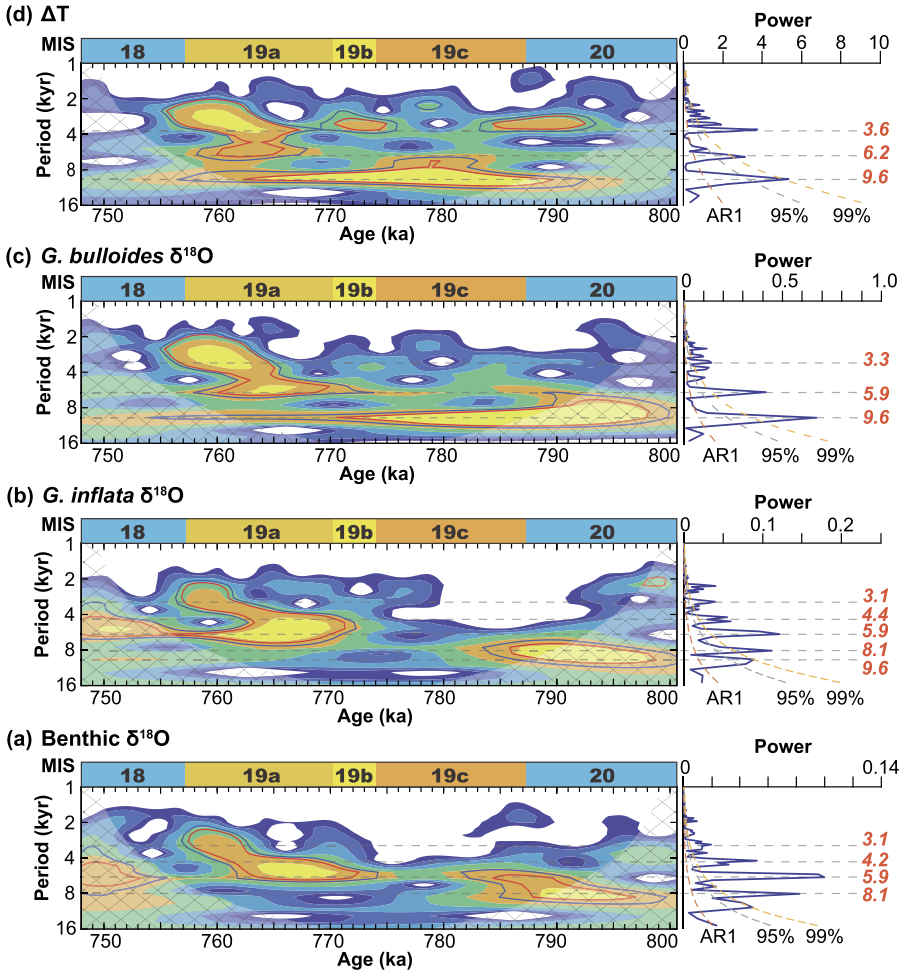

Fig. 4. Time series analysis results for millennial components of the $\delta^{18}O$ records from the CbCS. (a) Benthic $\delta^{18}O$. (b) $\delta^{18}O$ of *G. inflata*. (c) $\delta^{18}O$ of *G. bulloides*. (d) ΔT between surface and bottom water. The right panels show the spectral power obtained using the REDFIT method (Schulz and Mudelsee, 2002). The red, grey, and orange dashed lines designate the first-order autoregressive (AR1) red noise model fit, 95% confidence level, and 99% confidence level, respectively. The red numbers indicate periodicities over the 99% confidence level. The left panels show the local wavelet spectra of millennial components in the $\delta^{18}O$ and ΔT records from the CbCS obtained using the Morlet wavelet. The shade contours are at 0.5, 1.0, 2.0, 4.0, 8.0, and 16. The blue and red thick contours enclose regions with confidence levels greater than 90% and 95%, respectively. The cross-hatched regions indicate the cone of influence where the edge effect becomes important. MIS: marine isotope stage.

4.2. Power spectra of $\delta^{18}O$ and ΔT

Fig. 4 shows the results of spectral and wavelet analyses of the $\delta^{18}O$ and ΔT records. The power spectra of $\delta^{18}O_{Ben}$ and $\delta^{18}O_{inf}$, as well as $\delta^{18}O_{bul}$ show significant 5.9 kyr periodicity with confidence levels over 99%, which appear from MIS 19b in the wavelet power spectra with a confidence level over 90% with a gradual shortening trend toward MIS 18 (Figs. 4a–c). On the other hand, the wavelet power spectra of $\delta^{18}O_{bul}$ and ΔT show significant 9.6 kyr periodicity throughout MIS 19, with a confidence level of over 90% (Figs. 4c and 4d). The 5.9–6.2 kyr periodicity common to both the $\delta^{18}O$ and ΔT records and the 9.6 kyr periodicity of $\delta^{18}O_{bul}$ and ΔT are very similar to quarter (5.5 kyr) and half (10–12 kyr) precession cycles of insolation (Short et al., 1991; Berger et al., 2006).

5. Discussion

5.1. Millennial-scale variations in the CbCS

The large amplitudes of ΔT on a millennial scale during T-IX and the late MIS 19 were largely attributed to SST variations due to latitudinal displacements of the KEF. The maximum amplitude of the MIO in $\delta^{18}O_{bul}$ is 1.71‰, corresponding to a water temperature variation of 7.4 °C, and that of ΔT is 6.5 °C (Figs. 3c and d). A comparable SST increase of ~7–12.5 °C associated with a northward shift of the KEF and global climatic warming was observed during Termination I (T-I) from core MD01-2421, located ~100 km northeast of the CbCS (Fig. 1b; Yamamoto et al., 2005; Oba et al., 2006). On the other hand, in the Okhotsk Sea (cores PC-2 and PC-4), off the coast of southwest Japan (Cores St 14, St 19, and St 20) and in the Okinawa Trough (cores A7 and MD01-2404) far from the oceanic front (Fig. 1b), increases in SST were limited to ~3–4 °C across T-I (Sawada and Handa, 1998; Seki et al., 2004; Sun et al., 2005; Chen et al., 2010). Latitudinal displacement of oceanic fronts not only generates SST anomalies, but also changes the vertical thermal gradient in the ocean, as in modern observations (e.g., Kwon et al., 2010). These results indicate that pronounced variations in SST and vertical water temperature gradients during T-IX and the late MIS 19 reflect latitudinal displacements of the KEF. The increases in $\delta^{18}O$ and decreases in ΔT represent SST cooling and weakened stratification due to southward displacement of the KEF, and vice versa.

The $\delta^{18}O_{Ben}$ from the Kokusabata section is intermittently larger than that of the Yoro-Tabuchi and Yoro River sections, while the planktonic $\delta^{18}O$ profiles from both sections are generally con-

Please cite this article in press as: Haneda, Y., et al. Millennial-scale hydrographic changes in the northwestern Pacific during marine isotope stage 19: Teleconnections with ice melt in the North Atlantic. Earth Planet. Sci. Lett. (2019), https://doi.org/10.1016/j.epsl.2019.115936

sistent in amplitude and timing on a few-meter scale (millennial scale) variation (Fig. 2). The intermittent higher $\delta^{18}O_{Ben}$ values in the Kokusabata section up to ~0.2–0.4‰ are noticeable at stratigraphic intervals corresponding to the MIO-stadial periods. This implies that colder and/or saltier bottom water was advected in the Kokusabata section in association with southward displacements of the KEF.

The Kazusa Group has been interpreted as forearc basin fill, in which paleocurrents flowed from SW to NE where deeper sedimentary environments are observed (Katsura, 1984; Ito and Katsura, 1992). The depositional setting of the Kokumoto Formation observed in the Chiba section was deduced as a continental slope (Nishida et al., 2016). Since the gradient of continental slopes is generally more than 1:40 (e.g. Harff et al., 2016), the paleo-depth of the "downstream" Kokusabata section could be more than 100 meters deeper than that of the other "upstream" sections, according to the distance between them. Considering a thickness of the modern Kuroshio Current as less than 1000 m (Gallagher et al., 2015), the offset of $\delta^{18}O_{Ben}$ values between the Kokusabata and other sections is reasonably explained as follows. During the MIO-interstadial periods, a warm water mass reached over the depth of each section, due to northward displacement of the KEF. On the other hand, during the MIO-stadial periods, since a warm water mass had less influence on deeper sites due to the southward displacement of the KEF, the bottomwater temperature decreased more in the "deeper" Kokusabata section than the other sections. The $\delta^{18}O_{Ben}$ of the Kokusabata section between 20 and 25 m, corresponding to the interstadial period, is also higher than that of the Yoro-Tabuchi section (Fig. 2), because the magnitude of the northward displacement of the KEF would have been smaller than in other interstadial events.

5.2. Climatic teleconnection between the North Atlantic and northwestern Pacific

Fig. 3 compares the $\delta^{18}O$ and ΔT profiles from the CbCS with paleoceanographic records from the North Atlantic, which are benthic $\delta^{13}C$, ice-rafted debris (IRD), and $\%C_{37:4}$-based freshwater pulse records from Integrated Ocean Drilling Program (IODP) Site U1385 (Sánchez Goñi et al., 2016; Rodrigues et al., 2017) and ODP Site 980 (Wright and Flower, 2002). The benthic $\delta^{13}C$ records represent deep water ventilation associated with the ratio between ^{13}C-rich north-originating and ^{13}C-depleted south-originating deep waters. The relatively high $\delta^{13}C$ value suggests active formation of deep water in the North Atlantic bathed site and a strong AMOC, and vice versa (e.g., Ravelo and Hillaire-Marcel, 2007). $C_{37:4}$, the tetra-unsaturated alkenone with 37 carbon, is responsible for decreasing salinity in surface water and can be used to recognize events of massive cold freshwater input from iceberg melt or river discharge (Sánchez Goñi et al., 2016). The benthic $\delta^{13}C$ records from IODP U1385 and ODP 980 show a gradual decrease during MIS 20 and two minima are associated with two IRD peaks at 793 and 790 ka across T-IX. The benthic $\delta^{13}C$ records gradually increase from 788 ka during MIS 19c with no distinct IRD or freshwater inputs. The long-term ^{13}C enrichment, reflecting gradual AMOC enhancement, was terminated by a minor negative excursion of benthic $\delta^{13}C$ at 772 ka with the first IRD input and summer and winter SST declines at Site 980 (Fig. 3; Wright and Flower, 2002). Subsequently, benthic $\delta^{13}C$ profiles exhibit gradual AMOC weakening with three episodic negative $\delta^{13}C$ excursions, which co-occur with IRD peaks and freshwater pulses at 768.5, 763.5, and 759 ka (Figs. 3e and f). These episodic depletions of deep-water ventilation with iceberg and freshwater discharge into the North Atlantic represent abrupt AMOC disruptions or slowdowns associated with ice melting (Wright and Flower, 2002; Sánchez Goñi et al., 2016).

The five stadial periods across T-IX (YDt-1 at 791.0 ka, and YDt-2 at 787.7 ka) and during late MIS 19 (MIO-S2 at 766.5 ka, S3 at 761.7 ka, and S4 at 758.9 ka) are likely correlated with short-term AMOC disruptions and iceberg discharges at 793, 790, 768.5, 763.5, and 759 ka within the chronological uncertainty (Fig. 3). The ages and stratigraphic positions of the M–B boundary based on high-resolution paleomagnetic records and oxygen isotope stratigraphy from the CbCS (772.9 ka by Okada et al., 2017; Suganuma et al., 2018) and Site 980 (773.1 ka by Channell et al., 2010) support this correlation (Fig. 3). The quarter precession signal during the late MIS 19 has also been recognized in the freshwater pulse and benthic $\delta^{13}C$ record from IODP Site U1385 (Sánchez Goñi et al., 2016), the benthic $\delta^{18}O$ record from the Montalbano Jonico in southern Italy (Nomade et al., 2019), and the sediment $\delta^{18}O$ record from the Sulmona basin in central Italy (Regattieri et al., 2019), although the age models used in each study are independent of each other. These general consistencies in timing and periodicity indicate that southward displacements of the KEF in the northwestern Pacific were linked with the abrupt AMOC disruptions associated with freshwater forcing in the North Atlantic.

We propose the teleconnection of millennial-scale climate variations between the northwestern Pacific and North Atlantic, which were caused by the reorganization of atmospheric circulation due to AMOC disruption/reactivation (Fig. 5). Meltwater input into the subarctic North Atlantic causes AMOC weakening or shutdown, modulating the northward oceanic heat transport, which is associated with ocean surface freshening and stratification (e.g., Henry et al., 2016; Kawamura et al., 2017). The resulting disruption of heat redistribution immediately cools the Northern Hemisphere and gently warms the Southern Hemisphere ~400 yr afterwards via the thermal bipolar seesaw mechanism (e.g., Stocker and Johnsen, 2003; Kawamura et al., 2017). The resulting strong thermal contrast between the hemispheres causes southward displacement of the intertropical convergence zone (ITCZ) (Fig. 1a) associated with intensified trade winds and an asymmetric response of Hadley circulation (Fig. 5b; Broccoli et al., 2006; Asmerom et al., 2010; Kawamura et al., 2017). The ITCZ displacement accompanies parallel displacement and intensification of the mid-latitude prevailing westerlies associated with the deepening of the winter Aleutian Low via Rossby waves (Fig. 5b; Okumura et al., 2009; Asmerom et al., 2010). These atmospheric reorganizations immediately induce the KEF to be displaced southward and generate SST anomalies along the oceanic frontal zone via southward Ekman transport (Fig. 5b; Okumura et al., 2009; Kwon et al., 2010). After the end of the meltwater input, the AMOC is reinvigorated and redistributes heat and water from the Southern to the Northern Hemisphere. The recovery of the climate to the background state induces a northward shift of the ITCZ, westerlies, and the KEF (Fig. 5a; Okumura et al., 2009; Asmerom et al., 2010; Kawamura et al., 2017), which were amplified under the orbital configuration during MIS 19 (Suganuma et al., 2018). We conclude that these atmospheric dynamics due to freshwater forcing could have induced the southward/northward displacement of the KEF during T-IX and late MIS 19.

5.3. Equatorial insolation-paced climate variability

Our time series analysis results reveal a half precession cycle in the $\delta^{18}O_{bul}$ and ΔT profiles throughout MIS 19 (Figs. 4c and 4d). The half precession cycle in the wavelet power spectra is especially strong during MIS 19c, in which the IRD records from the North Atlantic exhibit minor or no iceberg discharge (e.g., Wright and Flower, 2002). Subsequently, more frequent periodicities, including the quarter precession cycle, appear from MIS 19b, although the half precession cycle still exists during the late MIS 19 in $\delta^{18}O_{bul}$

Please cite this article in press as: Haneda, Y., et al. Millennial-scale hydrographic changes in the northwestern Pacific during marine isotope stage 19: Teleconnections with ice melt in the North Atlantic. Earth Planet. Sci. Lett. (2019), https://doi.org/10.1016/j.epsl.2019.115936

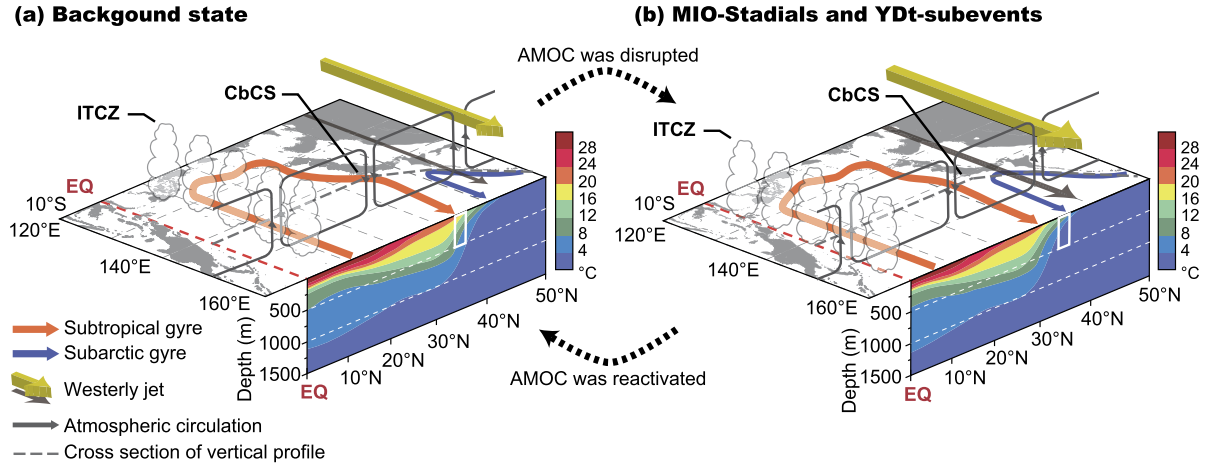

Fig. 5. Schematic representation of the relationship between latitudinal KEF shifts and atmospheric dynamics in the northwestern Pacific Ocean. (a) Hydrographic and atmospheric conditions in an active AMOC in the Atlantic Ocean based on present climatic conditions. (b) AMOC disruption in the Atlantic Ocean leading to southward shifts of the ITCZ and the westerly jet associated with intensified trade winds and the asymmetric response of Hadley circulation. The migration of the westerly jet led to a southward shift of the KEF and a shallowing of the thermocline depth in the CbCS. The latitudinal temperature profile is drawn based on a modern profile shown in Fig. S1d. The white boxes in the vertical temperature profiles indicate presumed water columns in the CbCS based on the δ^{18}O records. CbCS: Chiba composite section, EQ: equator, ITCZ: intertropical convergence zone.

and ΔT profiles (Figs. 4c and 4d). Therefore, half precession climate variability may have been independent of the ice melt and AMOC intensity variations in the North Atlantic, and may have paced the SST and vertical water temperature gradient variations in the CbCS during MIS 19.

Half precession cycles have been recognized in Pleistocene paleoceanographic and paleoclimatic records from the northwestern Atlantic (Weirauch et al., 2008; Billups and Scheiwald, 2014), mid-latitude North Atlantic (Ferretti et al., 2010, 2015), Chinese Loess Plateau (Sun and Huang, 2006), and northeastern Australia (Turney et al., 2004). The long-term planktonic δ^{18}O record from the northwestern Atlantic at ODP site 1058 contains intermittent quarter and half precession signals at least past 1350 ka across the mid-Pleistocene transition, in which the climate cycle transited from a 41-kyr to a quasi 100-kyr rhythm, and demonstrates that a half precession signal could have originated from the seasonality of low-latitude insolation (Weirauch et al., 2008; Billups and Scheiwald, 2014). The half precession signal is less obvious prior to 320 ka, but is intermittently apparent in the planktonic δ^{18}O record during several interglacial periods (Billups and Scheiwald, 2014). On the other hand, Ferretti et al. (2015) reported that the half precession signal in the planktonic δ^{18}O record from IODP Site U1313 in the North Atlantic was significant between 800 and 750 ka (its locality is shown in Fig. 1a). They concluded that half precession climate variability at Site U1313 was paced by insolation forcing at the equator when the perihelion of Earth's orbit coincides with the vernal or autumnal equinox. This combination, which occurs twice in every precession cycle, creates a second harmonic of the precession cycle in paleoceanographic and paleoclimatic records (Short et al., 1991; Berger et al., 2006; Ferretti et al., 2015).

Fig. 6 compares the half precession signals in the $\delta^{18}O_{bul}$ and ΔT profiles from the CbCS with equatorial insolation when the perihelion of the earth's orbit coincides with the vernal or autumnal equinox. We extracted the 10 kyr component curves from the $\delta^{18}O_{bul}$ and ΔT profiles using a Gaussian bandpass filter with a frequency of 0.10 kyr^{-1} and a bandwidth of 0.02 using the Analyseries software (Paillard et al., 1996). The 10 kyr component curves from both the $\delta^{18}O_{bul}$ and ΔT show maximum amplitudes at 784 ka and amplitude attenuations toward MIS 18. The evolution of equatorial insolation also shows a maximum amplitude at 783 ka with amplitude attenuation toward MIS 18 due to amplitude modulation by 400 kyr eccentricity forcing, and is well in phase with the 10 kyr $\delta^{18}O_{bul}$ and ΔT component curves. We propose the seasonality of low-latitude insolation paced sea surface variations in the CbCS throughout MIS 19, and that this low-latitude influence became larger when North Atlantic forcing was weak during MIS 19c.

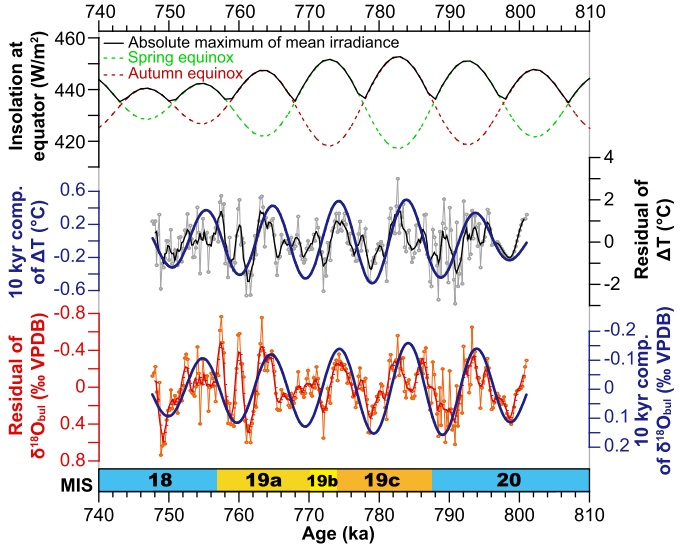

Fig. 6. Comparison of the temporal evolution of equatorial insolation and 10 kyr spectrum in ΔT and $\delta^{18}O_{bul}$ in the CbCS. (a) Insolation in equatorial regions at the spring (light green dashed line) and autumn (red dashed line) equinoxes (Laskar et al., 2004). The absolute maximum of the mean irradiance in the equatorial region at the spring and autumn equinoxes (thick black line) is also shown. (b) Millennial-scale component of ΔT from the CbCS (gray open circles and thin line), its 1000 yr moving average (black thick line), and its 10 kyr Gaussian bandpass filter output curve (thick blue line). (c) Millennial-scale component of $\delta^{18}O_{bul}$ from the CbCS (orange open circles and thin line), its 1000 yr moving average (black thick line), and its 10 kyr Gaussian bandpass filter output curve (thick blue line). MIS: marine isotope stage.

6. Conclusions

In this study, we provide new δ^{18}O records of the mean temporal resolution for 160 yr from late MIS 20 to early MIS 18

Please cite this article in press as: Haneda, Y., et al. Millennial-scale hydrographic changes in the northwestern Pacific during marine isotope stage 19: Teleconnections with ice melt in the North Atlantic. Earth Planet. Sci. Lett. (2019), https://doi.org/10.1016/j.epsl.2019.115936

using benthic and subsurface and surface planktonic foraminifers in addition to existing data from the CbCS on the Boso Peninsula, central Japan. The vertical water temperature structure and ΔT based on the $\delta^{18}O$ profiles exhibit latitudinal KEF oscillations during T-IX and the late MIS 19, which may have been associated with disruption/reactivation of the AMOC due to iceberg and freshwater discharge into the North Atlantic. The results of spectral and wavelet analyses show strong power spectra with 9600 yr periodicity in surface planktonic $\delta^{18}O$ and ΔT throughout MIS 19, which probably originated from the equatorial insolation at equinoxes coinciding with the orbital perihelion. The 9600 yr periodicity was especially strong during MIS 19c, whose paleoceanographic records from the North Atlantic show no or minor iceberg or freshwater discharge, indicating that the seasonality of low latitude insolation paced sea surface variations in the CbCS throughout MIS 19 and that this low latitude influence became larger when North Atlantic forcing by freshwater discharge and AMOC variability were low. Our results suggest that millennial-scale oceanographic variations and stability along the KEF under this orbital configuration are influenced by North Atlantic climate variability and tropical insolation forcing.

Acknowledgements

This study was supported by JSPS Kakenhi (Grants 16H04068, 15K13581, 17H06321, and 19H00710), the NIPR through an Advanced Project (KP306), a Sasakawa Scientific Research Grant from the Japan Science Society (29-625), a Geoscience Research Grant from the Tokyo Geographical Society, and Ministry of Education, Culture, Sports, Science and Technology, Japan (Rebuilding of Micropaleontological Reference Center collections, and Chemical stratigraphy and dating, for National Museum of Nature and Science). We thank Nozomi Suzuki and Kanako Mantoku for their support with the isotope analyses, the students of Ibaraki University for collecting the samples, and Prof. M.F. Sánchez Goñi for sharing the biomarker data from IODP Site U1385. We would like to thank Editage (www.editage.jp) for English language editing. We would also like to thank two reviewers and the editor of Earth and Planetary Science Letters for their constructive comments, which greatly improved the manuscript.

Appendix A. Supplementary material

Supplementary material related to this article can be found online at https://doi.org/10.1016/j.epsl.2019.115936.

References

Alvarez-Solas, J., Robinson, A., Montoya, M., Ritz, C., 2013. Iceberg discharges of the last glacial period driven by oceanic circulation changes. Proc. Natl. Acad. Sci. USA. https://doi.org/10.1073/pnas.1306622110.

Asmerom, Y., Polyak, V.J., Burns, S.J., 2010. Variable winter moisture in the southwestern United States linked to rapid glacial climate shifts. Nat. Geosci. 3, 113–117. https://doi.org/10.1038/ngeo754.

Berger, A., Loutre, M.F., Melice, J.L., 2006. Equatorial insolation: from precession harmonics to eccentricity frequencies. Clim. Past 2, 131–136. https://doi.org/10.5194/cp-2-131-2006.

Billups, K., Scheinwald, A., 2014. Origin of millennial-scale climate signals in the subtropical North Atlantic. Paleoceanography 29, 612–627. https://doi.org/10.1002/2014PA002641.

Bond, G., Broecker, W., Johnsen, S., McManus, J., Labeyrie, L., Jouzel, J., Bonani, G., 1993. Correlations between climate records from North Atlantic sediments and Greenland ice. Nature 365, 143–147.

Broccoli, A.J., Dahl, K.A., Stouffer, R., 2006. Response of the ITCZ to Northern Hemisphere cooling. Geophys. Res. Lett. 33, L01702. https://doi.org/10.1029/2005GL024546.

Channell, J.E.T., Hodell, D.A., Singer, B.S., Xuan, C., 2010. Reconciling astrochronological and $^{40}Ar/^{39}Ar$ ages for the Matuyama–Brunhes boundary and late Matuyama Chron. Geochem. Geophys. Geosyst. 11, Q0AA12. https://doi.org/10.1029/2010GC003203.

Chen, M.T., Lin, X.P., Chang, Y.P., Chen, Y.C., Lo, L., Shen, C.C., Yokoyama, Y., Oppo, D.W., Thompson, W.G., Zhang, R., 2010. Dynamic millennial-scale climate changes in the northwestern Pacific over the past 40,000 years. Geophys. Res. Lett. 37, L23603. https://doi.org/10.1029/2010GL045202.

Clement, A.C., Peterson, L.C., 2008. Mechanism of abrupt climate change of the last glacial period. Rev. Geophys. 46, RG4002. https://doi.org/10.1029/2006RG000204.

Dansgaard, W., Johnsen, S.J., Clausen, H.B., Dahl-Jensen, D., Gundestrup, N.S., Hammer, C.U., Hvidberg, C.S., Steffensen, J.P., Sveinbjornsdottir, A.E., Jouzel, J., Bond, G., 1993. Evidence for general instability of past climate form a 250-kyr ice-core record. Nature 364, 218–220. https://doi.org/10.1038/364218a0.

Elderfield, H., Ferretti, P., Greaves, M., Crowhurst, S., McCave, I.N., Hodell, D., Piotrowski, A.M., 2012. Evolution of ocean temperature and ice volume through the mid-Pleistocene climate transition. Science 337, 704–709. https://doi.org/10.1126/science.1221294.

Erez, J., Luz, B., 1983. Experimental paleotemperature equation for planktonic foraminifera. Geochim. Cosmochim. Acta 47, 1025–1031. https://doi.org/10.1016/0016-7037(83)90232-6.

Ferretti, P., Crowhurst, S.J., Hall, M.A., Cacho, I., 2010. North Atlantic millennial-scale climate variability 910 to 790 ka and the role of the equatorial insolation forcing. Earth Planet. Sci. Lett. 293, 28–41. https://doi.org/10.1016/j.epsl.2010.02.016.

Ferretti, P., Crowhurst, A.J., Naafs, B.D.A., Barbante, C., 2015. The Marine Isotope Stage 19 in the mid-latitude Northern Atlantic Ocean: astronomical signature and intra-interglacial variability. Quat. Sci. Rev. 108, 95–110.

Gallagher, S.J., Kitamura, A., Iryu, Y., Itaki, T., Koizumi, I., Hoiles, P.W., 2015. The Pliocene to recent history of the Kuroshio and Tsushima Currents: a multi-proxy approach. Prog. Earth Planet. Sci. 2, 17. https://doi.org/10.1186/s40645-015-0045-6.

Giaccio, B., Regattieri, E., Zanchetta, G., Nomade, S., Renne, P.R., Sprain, C.J., Drysdale, R.N., Tzedakis, P.C., Messina, P., Scardia, G., Sposato, A., Bassinot, F., 2015. Duration and dynamics of the best orbital analogue to the present interglacial. Geology 43, 603–606. https://doi.org/10.1130/G36677.1.

Hammer, Ø, Harper, D.A.T., Ryan, P.D., 2001. PAST: paleontological statistics software package for education and data analysis. Palaeontol. Electronica 4 (1), 9 pp.

Harff, J., Meschede, M., Petersen, S., Thiede, J., 2016. Encyclopedia of Marine Geosciences. Springer. ISBN 978-94-007-6239-8, 961 pp.

Heinrich, H., 1988. Origin and consequences of cyclic ice rafting in the Northeast Atlantic Ocean during past 130,000 years. Quat. Res. 29, 142–152. https://doi.org/10.1016/0033-5894(88)90057-9.

Henry, L.G., McManus, J.F., Curry, W.B., Roberts, N.L., Piotrowski, A.M., Keigwin, L.D., 2016. North Atlantic Ocean circulation and abrupt climate change during the last glaciation. Science 353, 470–474. https://doi.org/10.1126/science.aaf5529originally.

Hyodo, M., Bradak, B., Okada, M., Katoh, S., Kitaba, I., Dettman, D.L., Hayashi, H., Kumazawa, K., Hirose, K., Kazaoka, O., Shikoku, K., Kitamura, A., 2017. Millennial-scale northern Hemisphere Atlantic-Pacifc climate teleconnections in the earliest Middle Pleistocene. Sci. Rep. 7, 10036. https://doi.org/10.1038/s41598-017-10552-2.

Imai, M., Ebara, S., Kawashima, K., Kubo, N., Sato, N., Moriyama, E., 1988. Seasonal variation of chlorophyll-a in the seas around Japan. Oceanogr. Mag. 3 (1–2), 23–32.

Isono, D., Yamamoto, M., Irino, T., Oba, T., Murayama, M., Nakamura, T., Kawahata, H., 2009. The 1500-year climate oscillation in the midlatitude North Pacific during the Holocene. Geology 37, 591–594. https://doi.org/10.1130/G25667A.

Ito, M., Katsura, Y., 1992. Inferred glacio-eustatic control for high-frequency depositional sequences of the Plio-Pleistocene Kazusa Group, a forearc basin fill in Boso Peninsula, Japan. Sediment. Geol. 80, 67–75. https://doi.org/10.1016/0037-0738(92)90032-M.

Jonker, L., Kucera, M., 2015. Global analysis of seasonality in the shell flux of extant planktonic foraminifera. Biogeosciences 12, 2207–2226. https://doi.org/10.5194/bg-12-2207-2015.

Jouzel, J., Masson-Delmotte, V., Cattani, O., Dreyfus, G., Falourd, S., Hoffmann, G., Minster, B., Nouet, J., Barnola, J.M., Chappellaz, J., Fischer, H., Gallet, J.C., Johnsen, S., Leuenberger, M., Loulergue, L., Luethi, D., Oerter, H., Parrenin, F., Raisbeck, G., Raynaud, D., Schilt, A., Schwander, J., Selmo, E., Souchez, R., Spahni, R., Stauffer, B., Steffensen, J.P., Stenni, B., Stocker, T.F., Tison, J.L., Werner, M., Wolff, E.W., 2007. Orbital and millennial Antarctic climate variability over the past 800,000 years. Science 317, 793–796. https://doi.org/10.1126/science.1141038.

Katsura, Y., 1984. Depositional environments of the Plio-Pleistocene Kazusa Group, Boso Peninsula, Japan. In: Science Reports of the Institute of Geoscience. In: University of Tsukuba, Section B, Geological Sciences, vol. 5, pp. 69–104.

Kawamura, K., Abe-Ouchi, A., Motoyama, H., Ageta, Y., Aoki, S., Azuma, N., Fujii, Y., Fujita, K., Fujita, S., Fukui, K., Furukawa, T., Furusaki, A., Goto-Azuma, K., Greve, R., Hirabayashi, M., Hondoh, T., Hori, A., Horikawa, S., Horiuchi, K., Igarashi, M., Iizuka, Y., Kameda, T., Kanda, H., Kohno, M., Kuramoto, T., Matsushi, Y., Miyahara, M., Miyake, T., Miyamoto, A., Nagashima, Y., Nakayama, Y., Nakazawa, T., Nakazawa, F., Nishio, F., Obinata, I., Ohgaito, R., Oka, A., Okuno, J., Okuyama, J., Oyabu, I., Parrenin, F., Pattyn, F., Saito, F., Saito, T., Saito, T., Sakurai, T., Sasa, K., Seddik, H., Shibata, Y., Shinbori, K., Suzuki, K., Suzuki, T., Takahashi, A., Taka-

hashi, K., Takahashi, S., Takata, M., Tanaka, Y., Uemura, R., Watanabe, G., Watanabe, O., Yamasaki, T., Yokoyama, K., Yoshimori, M., Yoshimoto, T., 2017. State dependence of climatic instability over the past 720,000 years from Antarctic ice cores and climate modeling. Sci. Adv. 3, e1600446.

Kida, S., Mitsudera, H., Aoki, S., Guo, X., Ito, S., Kobashi, F., Komori, N., Kubokawa, A., Miyama, T., Morie, R., Nakamura, H., Nakamura, T., Nakano, H., Nishigaki, H., Nonaka, M., Sasaki, H., Sasaki, Y.N., Suga, T., Sugimoto, S., Taguchi, B., Takaya, K., Tozuka, T., Tsujino, H., Usui, N., 2016. Oceanic fronts and jets around Japan: a review. In: Nakamura, H., Isobe, A., Minibe, S., Mitsudera, H., Nonaka, M., Suga, T. (Eds.), "Hot Spots" in the Climate System. Springer Japan, pp. 1–30.

Kleiven, H.F., Hall, I.R., McCave, I.N., Knorr, G., Jansen, E., 2011. Coupled deep-water flow and climate variability in the Middle Pleistocene North Atlantic. Geology 39, 343–346. https://doi.org/10.1130/G31651.1.

Kwon, Y.O., Alexander, M.A., Bond, N.A., Frankignoul, C., Nakamura, H., Qiu, B., Thompson, L., 2010. Role of the gulf stream and Kuroshio–Oyashio systems in large-scale atmosphere–ocean interaction: a review. J. Climate 23, 3249–3281. https://doi.org/10.1175/2010JCLI3343.1.

Laskar, J., Robutel, P., Joutel, F., Gastineau, M., Correia, A., Levrard, B., 2004. A long term numerical solution for the insolation quantities of the Earth. Astron. Astrophys. 428, 261–285.

Lisiecki, L.E., Raymo, M.E., 2005. A Pliocene-Pleistocene stack of 57 globally distributed benthic $\delta^{18}O$ records. Paleoceanography 20, PA1003. https://doi.org/10.1029/2004PA001071.

Locarnini, R.A., Mishonov, A.V., Antonov, J.I., Boyer, T.P., Garcia, H.E., Baranova, O.K., Zweng, M.M., Paver, C.R., Reagan, J.R., Johnson, D.R., Hamilton, M., Seidov, D., 2013. World Ocean Atlas 2013, vol. 1: Temperature. Levitus, S. (Ed.), Mishonov, A. (Technical Ed.), NOAA Atlas NESDIS, vol. 73, 40 pp.

Menviel, L., Timmermann, A., Friedrich, T., England, M.H., 2014. Hindcasting the continuum of Dansgaard–Oeschger variability: mechanisms, patterns and timing. Clim. Past 10, 63–77. https://doi.org/10.5194/cp-10-63-2014.

Nishida, N., Kazaoka, O., Izumi, K., Suganuma, Y., Okada, M., Yoshida, T., Ogitsu, I., Nakazato, H., Kameyama, S., Kagawa, A., Morisaki, M., Nirei, H., 2016. Sedimentary processes and depositional environments of a continuous marine succession across the Lower–Middle Pleistocene boundary: Kokumoto Formation, Kazusa group, central Japan. Quat. Int. 397, 3–15. https://doi.org/10.1016/j.quaint.2015.06.045.

Nomade, S., Bassinot, F., Marino, M., Simon, Q., Dewilde, F., Maiorano, P., Isguder, G., Blamart, D., Girone, A., Scao, V., Pereira, A., Toti, F., Bertini, A., Combourieu-Nebout, N., Peral, M., Bourles, D.L., Petrosino, P., Gallicchio, S., Ciaranfi, N., 2019. High-resolution foraminifer stable isotope record of MIS 19 at Montalbano Jonico, southern Italy: a window into Mediterranean climatic variability during a low-eccentricity interglacial. Quat. Sci. Rev. 205, 106–125. https://doi.org/10.1016/j.quascirev.2018.12.008.

Oba, T., Irino, T., Yamamoto, M., Murayama, M., Takamura, A., Aoki, K., 2006. Paleoceanographic change off central Japan since the last 144,000 years based on high-resolution oxygen and carbon isotope records. Glob. Planet. Change 53, 5–20. https://doi.org/10.1016/j.gloplacha.2006.05.002.

Okada, M., Suganuma, Y., Haneda, Y., Kazaoka, O., 2017. Paleomagnetic direction and paleointensity variations during the Matuyama–Brunhes polarity transition from a marine succession in the Chiba composite section of the Boso Peninsula, central Japan. Earth Planets Space 69, 1–19.

Okumura, Y., Deser, C., Hu, A., Timmermann, A., Xie, S.P., 2009. North Pacific climate response to freshwater forcing in the subarctic North Atlantic: oceanic and atmospheric pathways. J. Climate 22, 1424–1445. https://doi.org/10.1175/2008JCLI2511.1.

Paillard, D.L., Labeyrie, L., Yiou, P., 1996. Macintosh program performs time-series analysis. Eos Trans. AGU 77, 379. https://doi.org/10.1029/96EO00259.

Prokopenko, A.A., Hinnov, L.A., Williams, D.F., Kuzmin, M.I., 2006. Orbital forcing of continental climate during the Pleistocene: a complete astronomically tunedclimatic record from Lake Baikal, SE Siberia. Quat. Sci. Rev. 25, 3431–3457. https://doi.org/10.1016/j.quascirev.2006.10.002.

Qiu, B., 2001. Kuroshio and Oyashio currents. In: Steele, J.H., Thorpe, S.A., Turekian, K.K. (Eds.), Encyclopedia of Ocean Sciences. Academic, London, pp. 1413–1425.

Railsback, L.B., Gibbard, P.L., Head, M.J., Voarintsoa, N.R.G., Toucanne, S., 2015. An optimized scheme of lettered marine isotope substages for the last 1.0 million years, and the climatostratigraphic nature of isotope stages and substages. Quat. Sci. Rev. 111, 94–106. https://doi.org/10.1016/j.quascirev.2015.01.012.

Ravelo, A.C., Hillaire-Marcel, C., 2007. The use of oxygen and carbon isotopes of foraminifera in paleoceanography. In: Hillaire-Marcel, C., De Vernal, A. (Eds.), Proxies in Late Cenozoic Paleoceanography. Elsevier, Oxford, pp. 735–764.

Regattieri, E., Giaccio, B., Mannella, G., Zanchetta, G., Nomade, S., Tognarelli, A., Perchiazzi, N., Vogel, H., Boschi, C., Drysdale, R.N., Wagner, B., Gemelli, M., Tzedakis, P., 2019. Frequency and dynamics of millennial-scale variability during Marine Isotope Stage 19: insights from the Sulmona Basin (central Italy). Quat. Sci. Rev. 214, 28–43. https://doi.org/10.1016/j.quascirev.2019.04.024.

Rodrigues, T., Alonso-García, M., Hodell, D.A., Rufino, M., Naughton, F., Grimalt, J.O., Voelker, A.H.L., Abrantes, F., 2017. A 1-Ma record of sea surface temperature and extreme cooling events in the North Atlantic: a perspective from the Iberian Margin. Quat. Sci. Rev. 172, 118–130.

Sagawa, T., Yokoyama, Y., Ikehara, M., Kuwae, M., 2011. Vertical thermal structure history in the western subtropical North Pacific since the last glacial maximum. Geophys. Res. Lett. 38, L00F02. https://doi.org/10.1029/2010GL045827.

Sánchez Goñi, M.F., Rodrigues, T., Hodell, D.A., Polanco-Martínez, J.M., Alonso-García, M., Hernández-Almeida, I., Desprat, S., Ferretti, P., 2016. Tropically-driven climate shifts in southwestern Europe during MIS19, a low eccentricity interglacial. Earth Planet. Sci. Lett. 448, 81–93. https://doi.org/10.1016/j.epsl.2016.05.018.

Sawada, K., Handa, N., 1998. Variability of the path of the Kuroshio ocean current over the past 25,000 years. Nature 392, 592–595. https://doi.org/10.1038/33391.

Schiebel, R., Hemleben, C., 2017. Planktic Foraminifers in the Modern Ocean. Springer, Heidelberg. 358 pp.

Schlitzer, R., 2015. Ocean data view. http://odv.awi.de.

Schulz, M., Mudelsee, M., 2002. REDFIT: estimatingred-noise spectra directly from unevenly spaced paleoclimatic time series. Comput. Geosci. 28, 421–426.

Seki, O., Kawamura, K., Ikehara, M., Nakatsuka, T., Oba, T., 2004. Variation of alkenone sea surface temperature in the Sea of Okhotsk over the last 85 kyrs. Org. Geochem. 35, 347–354.

Short, D.A., Mengel, J.D., Crowley, T.J., Hyde, W.T., North, G.R., 1991. Filtering of Milankovitch cycles by Earth's geography. Quat. Res. 35, 157–173. https://doi.org/10.1016/0033-5894(91)90064-C.

Simon, Q., Bourles, D.L., Bassinot, F., Nomade, S., Marino, M., Ciaranfi, N., Girone, A., Maiorano, P., Thouveny, N., Choy, S., Dewilde, F., Scao, V., Isguder, G., Blamart, D., 2017. Authigenic $^{10}Be/^{9}Be$ ratio signature of the Matuyama-Brunhes boundary in the Montalbano Jonico marine succession. Earth Planet. Sci. Lett. 460, 255–267. https://doi.org/10.1016/j.epsl.2016.11.052.

Simon, Q., Suganuma, Y., Okada, M., Haneda, Y., 2019. ASTER team. High-resolution ^{10}Be and paleomagnetic recording of the last polarity reversal in the Chiba composite section: age and dynamics of the Matuyama–Brunhes transition. Earth Planet. Sci. Lett. 519, 92–100. https://doi.org/10.1016/j.epsl.2019.05.004.

Stocker, T.F., Johnsen, S.J., 2003. A minimum thermodynamic model for the bipolar seesaw. Paleoceanography 18, 1087. https://doi.org/10.1029/2003PA000920.

Suganuma, Y., Okada, M., Horie, K., Kaiden, H., Takehara, M., Senda, R., Kimura, J., Kawamura, K., Haneda, Y., Kazaoka, O., Head, J.M., 2015. Age of Matuyama-Brunhes boundary constrained by U-Pb zircon dating of a widespread tephra. Geology 43, 491–494. https://doi.org/10.1130/G36625.1.

Suganuma, Y., Haneda, Y., Kameo, K., Kubota, Y., Hayashi, H., Itaki, T., Okuda, M., Head, M.J., Sugaya, M., Nakzato, H., Igarashi, A., Shikoku, K., Hongo, M., Watanabe, M., Satoguchi, Y., Takeshita, Y., Nishida, N., Izumi, K., Kawamura, K., Kawamata, M., Okuno, J., Yoshida, T., Ogitsu, I., Yabusaki, H., Okada, M., 2018. Paleoclimatic and paleoceanographic records of Marine Isotope Stage 19 at the Chiba composite section, central Japan: a reference for the Early-Middle Pleisotocene boundary. Quat. Sci. Rev. 191, 406–430.

Sun, J., Huang, X., 2006. Half-precessional cycles recorded in Chinese loess: response to low-latitude insolation forcing during the last interglaciation. Quat. Sci. Rev. 25, 1065–1072.

Sun, Y., Oppo, D.W., Xiang, R., Liu, W., Gao, S., 2005. Last deglaciation in the Okinawa Trough: subtropical northwest Pacific link to Northern Hemisphere and tropical climate. Paleoceanography 20, PA4005. https://doi.org/10.1029/2004PA001061.

Taguchi, B., Nakamura, H., Nonaka, M., Komori, N., Kuwano-Yoshida, A., Takaya, K., Goto, A., 2012. Seasonal evolution of atmospheric response to decadal SST anomalies in the North Pacific subarctic frontal zone: observations and a coupled model simulation. J. Climate 25, 111 111e.

Tanaka, I., Hyodo, M., Ueno, Y., Kitaba, I., Sato, H., 2017. High-resolution diatom record of paleoceanographic variations across the Early-Middle Pleistocene boundary in the Chiba Section, central Japan. Quat. Int. 455, 141–148. https://doi.org/10.1016/j.quaint.2017.08.017.

Torrence, C., Compo, G.P., 1998. A practical guide to wavelet analysis. Bull. Am. Meteorol. Soc. 79, 61–78. Wavelet software is available at http://paos.colorado.edu/research/wavelets/.

Turney, C.S.M., Kershaw, A.P., Clemens, S.C., Branch, N., Moss, P.T., Fifield, L.K., 2004. Millennial and orbital variations of El Niño/Southern Oscillation and high-latitude climate in the last glacial period. Nature 428, 306–310. https://doi.org/10.1038/nature02386.

Tzedakis, P.C., Channell, J.E.T., Hodell, D.A., Kleiven, H.F., Skinner, L.C., 2012. Determining the natural length of the current interglacial. Nat. Geosci. 5, 138–141. https://doi.org/10.1038/ngeo1358.

Valet, J.P., Bassinot, F., Bouilloux, A., Bourles, D., Nomade, S., Guillou, V., Lopes, F., Thouveny, N., Dewilde, F., 2014. Geomagnetic, cosmogenic and climatic changes across the last geomagnetic reversal from equatorial Indian Ocean sediments. Earth Planet. Sci. Lett. 397, 67–79. https://doi.org/10.1016/j.epsl.2014.03.053.

Valet, J.P., Bassinot, F., Simon, Q., Savranskaia, T., Thouveny, N., Bourlés, D.L., Villedieu, A., 2019. Constraining the age of the last geomagnetic reversal from geochemical and magnetic analyses of Atlantic, Indian, and Pacific Ocean sediments. Earth Planet. Sci. Lett. 506, 323–331. https://doi.org/10.1016/j.epsl.2018.11.012.

Weirauch, D., Billups, K., Martin, P., 2008. Evolution of millennial-scale climate variability during the mid-Pleistocene. Paleoceanography 23, PA3216. https://doi.org/10.1029/2007PA001584.

Please cite this article in press as: Haneda, Y., et al. Millennial-scale hydrographic changes in the northwestern Pacific during marine isotope stage 19: Teleconnections with ice melt in the North Atlantic. Earth Planet. Sci. Lett. (2019), https://doi.org/10.1016/j.epsl.2019.115936

Wennrich, V., Minyuk, P.S., Borkhodoev, V., Francke, A., Ritter, B., Nowaczyk, N.R., Sauerbrey, M.A., Brigham-Grette, J., Melles, M., 2014. Pliocene to Pleistocene climate and environmental history of Lake El'gygytgyn, Far East Russian Arctic, based on high-resolution inorganic geochemistry data. Clim. Past 10, 1381–1399. https://doi.org/10.5194/cp-10-1381-2014.

Wright, A.K., Flower, B.J., 2002. Surface and deep ocean circulation in the subpolar North Atlantic during the mid-Pleistocene revolution. Paleoceanography 17, 1068. https://doi.org/10.1029/2002PA000782.

Xu, X., Oda, M., 1999. Surface-water evolution of the eastern East China Sea during the last 36,000 years. Mar. Geol. 156, 285–304. https://doi.org/10.1016/S0025-3227(98)00183-2.

Xu, X., Yamasaki, M., Oda, M., Honda, M., 2005. Comparison of seasonal flux variations of planktonic foraminifera in sediment traps on both sides of the Ryukyu Islands, Japan. Mar. Micropaleontol. 58, 45–55. https://doi.org/10.1016/j.marmicro.2005.09.002.

Yamamoto, M., Suemune, R., Oba, T., 2005. Equatorward shift of the subarctic boundary in the northwestern Pacific during the last deglaciation. Geophys. Res. Lett. 32, 1–4. https://doi.org/10.1029/2004GL021903.

Yamasaki, M., Oda, M., 2003. Sedimentation of planktonic foraminifera in the East China Sea: evidence from a sediment trap experiment. Mar. Micropaleontol. 49, 3–20. https://doi.org/10.1016/S0377-8398(03)00024-0.

Yamasaki, M., Murakami, T., Tsuchihashi, M., Oda, M., 2010. Seasonal variation in living planktic foraminiferal assemblage in the northeastern part of the East China Sea. Fossils (Kaseki) 87, 35–46 (in Japanese with English abstruct).

Zweng, M.M., Reagan, J.R., Antonov, J.I., Locarnini, R.A., Mishonov, A.V., Boyer, T.P., Garcia, H.E., Baranova, O.K., Johnson, D.R., Seidov, D., Biddle, M.M., 2013. World Ocean Atlas 2013, vol. 2: Salinity. Levitus, S. (Ed.), Mishonov, A. (Technical Ed.), In: Levitus, S. (Ed.), A. Mishonov Technical Ed., NOAA Atlas NESDIS, vol. 74, 39 pp.

Please cite this article in press as: Haneda, Y., et al. Millennial-scale hydrographic changes in the northwestern Pacific during marine isotope stage 19: Teleconnections with ice melt in the North Atlantic. Earth Planet. Sci. Lett. (2019), https://doi.org/10.1016/j.epsl.2019.115936